Chapter 2

Small-pore Molecular Sieves and MTO Reaction

In this chapter, the experimental part (syntheses, characterizations, and MTO reactions of molecular sieves) of Part I of my thesis is presented. This chapter and the next chapter (Chapter III) are combined reconstitutions of two of my publications: J. H. Kang et al., ChemPhysChem 2018, 19, 412 and J. H. Kang et al., ACS Catal. 2019, DOI: 10.1021/acscatal.9b00746. The majority of this chapter is adapted from the Supporting Information (methods and characterization) of my ACS Catalysis paper, but further augmented with the contents from my ChemPhysChem paper.

2.1. Introduction

The MTO reaction over small-pore/cage-type molecular sieves is a promising technology which can meet the ever-increasing light olefin demands.[8, 13, 49] Methanol can be synthesized from syngas which can be obtained from various non-petroleum sources such as coal and natural gas.[9] The commercialized catalyst for the MTO process is SAPO-34, an $AlPO_4$-based molecular sieve solid acid having a CHA topology.[11] The cage of CHA can effectively trap bulky hydrocarbon pool intermediates and let methanol and light olefins diffuse through its pore openings consisting of 8 tetrahedral atoms. This cage structure of SAPO-34 is the origin of its high selectivity (80–90%) toward light olefins (ethylene and propylene). The first and largest coal-to-olefin plant was constructed in Inner Mongolia in 2010 on the basis of the DMTO process by DICP.[13]

There is a scientific consensus that the mechanism of MTO reaction is based on the hydrocarbon pool cycles (shown in the previous chapter) of various polymethyl aromatic intermediates which are active under the reaction condition.[8, 27] There has been a recognition that the cage structures dictate types of intermediates formed during the reaction.[23, 50] During the recent decade, on the basis of advanced characterization techniques such as the *in situ* solid state nuclear magnetic resonance (NMR) spectroscopy, hydrocarbon pool intermediates formed within cages could be identified.[1] It was confirmed that the types of polymethyl aromatic intermediates are actually controlled by the cage geometry.[32-34, 36, 46] Also, many attempts were made to correlate the cage structure with the olefin product distributions.[32, 38-39, 41, 46] Despite these efforts, the global shape selectivity of the MTO reaction has not yet established.

To establish a general rule regarding the shape selectivity, the reaction condition should be controlled first. The reaction temperature is the most important variable that determines the regime of MTO mechanism, and significantly affects the olefin selectivity distributions.[13, 32, 46] However, many of the previously reported experiments were performed at different temperatures among which a solid comparison is hard to be made. 350 °C[40, 42-43, 51] and 425 °C[44, 52] were the most frequently adopted reaction temperatures other than 400 °C. Furthermore, the number of studied topologies must be as many as possible. Most of the previous studies compared less than 5 topologies. To deduce a valid statement about the shape selectivity, a wide array of molecular sieves having various topologies and compositions must be tested in the same reaction condition. For this reason, in this work, the reaction temperature and the weight-hourly space volume of methanol were strictly controlled at 400 °C and 1.3 h^{-1}.

The molecular sieves tested in this work were selected as follows. Among 245 frameworks which have been discovered up to date, only 34 frameworks have cage structures bounded with 8-ring pore windows.[16] Of course, not all of these frameworks are applicable to the MTO reaction. Some topologies have been realized only as pure-silica which has no acid site. A topology like tschörtnerite (TSC) has never been realized as aluminosilicates having a Si/Al ratio higher than 1.[53-54] Zeolites having low Si/Al ratios (e.g., less than 3) show too short lifetime to obtain meaningful numbers of data points of nearly complete methanol conversion (i.e., over 98%) due to high paired-site density.[64] For zeolites, it is important to have moderate-range Si/Al ratios (ca. Si/Al = 4–30) to show optimal MTO activities. Therefore, frameworks having 'MTO-unfeasible' elemental compositions were eliminated from the list. Some frameworks have cages which are also present in other frameworks. For example, AFT have CHA and AFX cages, and AFV have CHA and LEV cages.[16, 55-56] Since CHA, AFX, and LEV are already on the list, to avoid redundancy, these types of 'combined-cage' topologies were also ruled out. Frameworks which have elemental compositions not zeolitic neither $AlPO_4$-based, such as NPT, were removed.[57] Finally, 14 frameworks (CHA, AFX, SFW, ERI, LEV, AEI, DDR, ITE, RTH, SAV, LTA, RHO, KFI, UFI) were selected as shown in Figure 2.1. These frameworks were reproduced as zeolites and/or SAPOs/MAPOs in this work. On the top of this list, three zeolites (SSZ-104, SSZ-99, and SSZ-105) having disordered structures of intergrown phases and one zeolite having novel topology (SSZ-27) were provided by Chevron.

Finally, the MTO reactions of the following 30 small-pore/cage-type molecular sieves were investigated: SSZ-13 (CHA), SAPO-34 (CHA), CoAPO-34 (CHA), MgAPO-34 (CHA), SSZ-16 (AFX), SAPO-56 (AFX), SSZ-52 (SFW), STA-18 (SFW), SSZ-99 (CHA/GME intergrowth), SSZ-104 (CHA/ABC-6-type disordered), SSZ-27, Nu-3 (SSZ-17, LEV), SAPO-35 (LEV), SSZ-98 (ERI), SSZ-105 (LEV/ERI intergrowth), SSZ-39 (AEI), SAPO-18 (AEI), CoAPO-18 (AEI), MgAPO-18 (AEI), SSZ-28 (DDR), Zeolite RTH (SSZ-50), Zeolite ITE (ITQ-3), STA-7 (SAV), Zeolite LTA, SAPO-42 (LTA), Zeolite RHO, DNL-6 (RHO), Zeolite KFI, STA-14 (KFI), and UZM-5 (UFI). In this chapter, the syntheses and characterizations of OSDAs and molecular-sieve catalysts are presented. The results of MTO reactions over catalysts listed above were depicted as the time-on-stream charts. MTO behaviors of these catalysts were analyzed focusing on their transient trends.

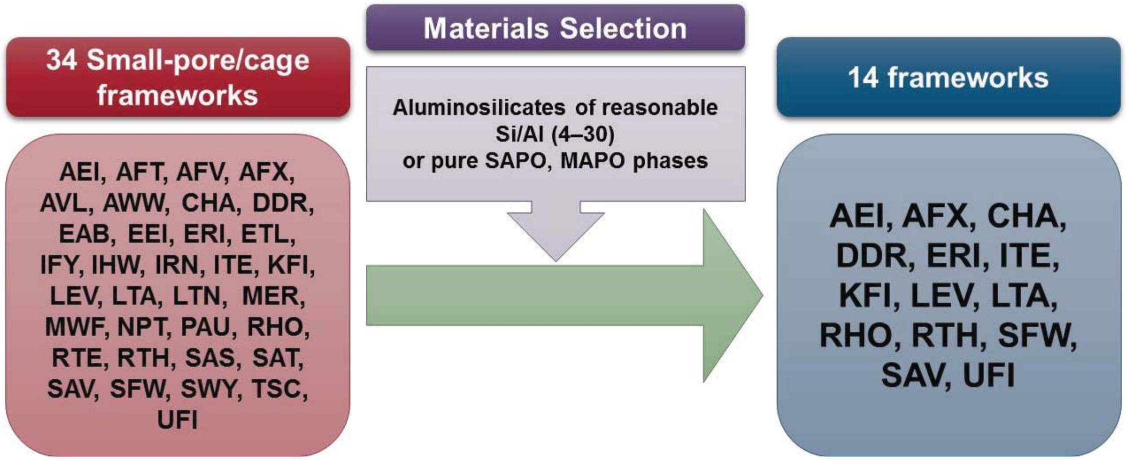

Figure 2.1. Selection of topologies.

2.2. Experimental

2.2.1. Synthesis of Organic Structure-Directing Agents

Materials 1,4-diazabicyclo[2.2.2]octane (DABCO, 99%, Sigma-Aldrich), 1,6-dibromohexane (98%, Sigma-Aldrich), quinuclidine (97%, Alfa Aesar), N-methylpiperidine (99%, Sigma-Aldrich), methyl iodide (99.5%, Cu-stabilized Sigma-Aldrich), 1,2,4,5-tetramethylimidazole (98%, TCI Chemical), 1,2-dimethylimidazole (98%, Sigma-Aldrich), 4-methylbenzyl chloride (98%, Sigma-Aldrich) were used as-received without further purification.

Organic Syntheses The quaternary ammonium OSDAs used in this work were prepared as their halide forms firstly by the S_N2 reactions stated below. The reaction schemes for preparation of the OSDAs are demonstrated in Figure 2.2.

1,1’-(hexane-1,6-diyl)bis(1,4-diazabicyclo[2.2.2]octanium) dibromide (C_6-diDABCO-Br_2) was prepared from the S_N2 reaction of DABCO and 1,6-dibromohexane.[58] (Figure 2.2(a)) DABCO (67.3 g, 600 mmol, excess) was dissolved in 200 mL of methanol in a 500 ml round-bottom flask, and the solution was heated up to 45 °C. A 50-mL dropping funnel was charged with 1,6-dibromohexane (24.4 g, 100 mmol) dissolved in 100 mL of methanol. The 1,6-dibromohaxane solution was slowly added to the DABCO solution dropwise for 30 min while vigorously stirring to prevent the possible oligomerization. The reaction mixture was heated up to the reflux temperature and stirred for 24 hours. After that, the solvent was evaporated using a rotary evaporator. The white solid product was repeatedly washed with an amount of diethyl ether (1 L) to wash out excess DABCO. The product was dried in a vacuum at room temperature. ^1H NMR (500 MHz, D_2O): δ 3.34 (t, 12H), 3.21 (m, 4H), 3.12 (t, 12H), 1.73 (m, 4H), 1.37 (m, 4H). ^{13}C NMR (125 MHz, D_2O): δ 64.27, 52.05, 44.16, 25.12, 21.05.

N-methylquinuclidinium iodide was prepared from the S_N2 reaction of quinuclidine and methyl iodide.[59] (Figure 2.2(b)) 10 g (90 mmol) of quinuclidine was dissolved in 150 mL of chloroform in a 500-mL round-bottom flask, and cooled down using a dry-ice bath. A 50-mL dropping funnel was separately filled with 11.2 mL of methyl iodide (25.5 g, 180 mmol). Methyl iodide was added dropwise to the cooled quinuclidine-chloroform solution slowly because the reaction is highly exothermic. Methyl iodide must be handled in a well-ventilated fume hood because it is very volatile (b.p., 42.4 °C) and toxic if accidentally inhaled. After that, the reaction mixture was stirred at room temperature for extra 72 hours. Solvent and excess methyl iodide were evaporated using a rotary evaporator. Appropriate personal protective equipment (PPE) must be used since toxic vapor containing methyl iodide is generated. The solid product was repeatedly washed with an amount of diethyl ether (1 L). The product was dried in a vacuum at room temperature. ^1H NMR (500 MHz, $CDCl_3$): δ 3.83 (t, 6H), 3.36 (s, 3H), 2.33 (septet, 1H), 2.10 (m, 6H). ^{13}C NMR (125 MHz, D_2O): δ 56.90, 51.83, 23.42, 18.57.

N,N'-dimethyl-1,4-diazabicyclo[2.2.2]octanium diiodide (DMDABCO^{2+}(I$^-$)$_2$), N,N'-dimethylpiperidinium iodide (DMP$^+$I$^-$), 1,2,3,4,5-pentamethylimidazolium iodide (PMI$^+$I$^-$) were prepared from the S$_N$2 reactions shown in Figure 2.2(c–e).[48, 60-61] Synthesis protocols for these OSDAs are analogous to the method for N-quinuclidinium iodide explained above, except for the reactant amines. For DMDABCO^{2+}, 16.8 g (150 mmol) of DABCO and 85.2 g (600 mmol) of methyl iodide were used: ^{1}H NMR (500 MHz, D$_2$O): δ 4.68 (s, 6H), 3.44 (s, 12H). ^{13}C NMR (125 MHz, D$_2$O): δ 53.45, 44.38. For DMP^{2+}, 9.2 g (100 mmol) of N-methylpiperidine and 42.6 g (300 mmol) of methyl iodide were used. ^{1}H NMR (500 MHz, CD$_3$OD): δ 3.54 (t, 4H), 3.27 (s, 6H), 2.00 (m, 4H), 1.78 (qnt, 2H). ^{13}C NMR (125 MHz, CD$_3$OD): δ 62.59, 51.25, 20.44, 19.96. For PMI$^+$, 18.7 g (150 mmol) of 1,2,4,5-tetramethylimidazole and 63.9 g (450 mmol) of methyl iodide were used. ^{1}H NMR (500 MHz, D$_2$O): δ 3.51 (s, 6H), 2.43 (s, 3H), 2.10 (s, 6H). ^{13}C NMR (125 MHz, D$_2$O): δ 142.06, 125.24, 31.26, 9.39, 7.68.

1,2-dimethyl-3-(4-methylbenzyl)imidazolium chloride (12DM34MBI$^+$Cl$^-$) was synthesized from the S$_N$2 reaction between 1,2-dimethylimidazolium and 4-methylbenzyl chloride.[62-63] 14.4 g of 1,2-dimethylimidazoilium (150 mmol) was dissolved in 200 ml of toluene. 21.1 g of 4-methylbenzyl chloride (150 mmol) was added slowly. The reaction mixture was heated to 105 °C and the reaction proceeded for 24 hours. After that, the mixture was cooled down to room temperature, and the light yellowish solid was collected by filtration, and washed with a copious amount of diethyl ether (1 L) and dried in a vacuum at room temperature. ^{1}H NMR (500 MHz, D$_2$O): δ 7.18 (dd, 2H), 7.13 (d, 2H), 7.05 (d, 2H), 6.50 (s, 2H), 3.61 (s, 3H), 2.41 (s, 3H), 2.18 (s, 3H). 13C NMR (125 MHz D$_2$O): δ 144.14, 139.16, 130.64, 129.67, 127.68, 122.15, 120.89, 51.10, 34.49, 20.07, 8.93.

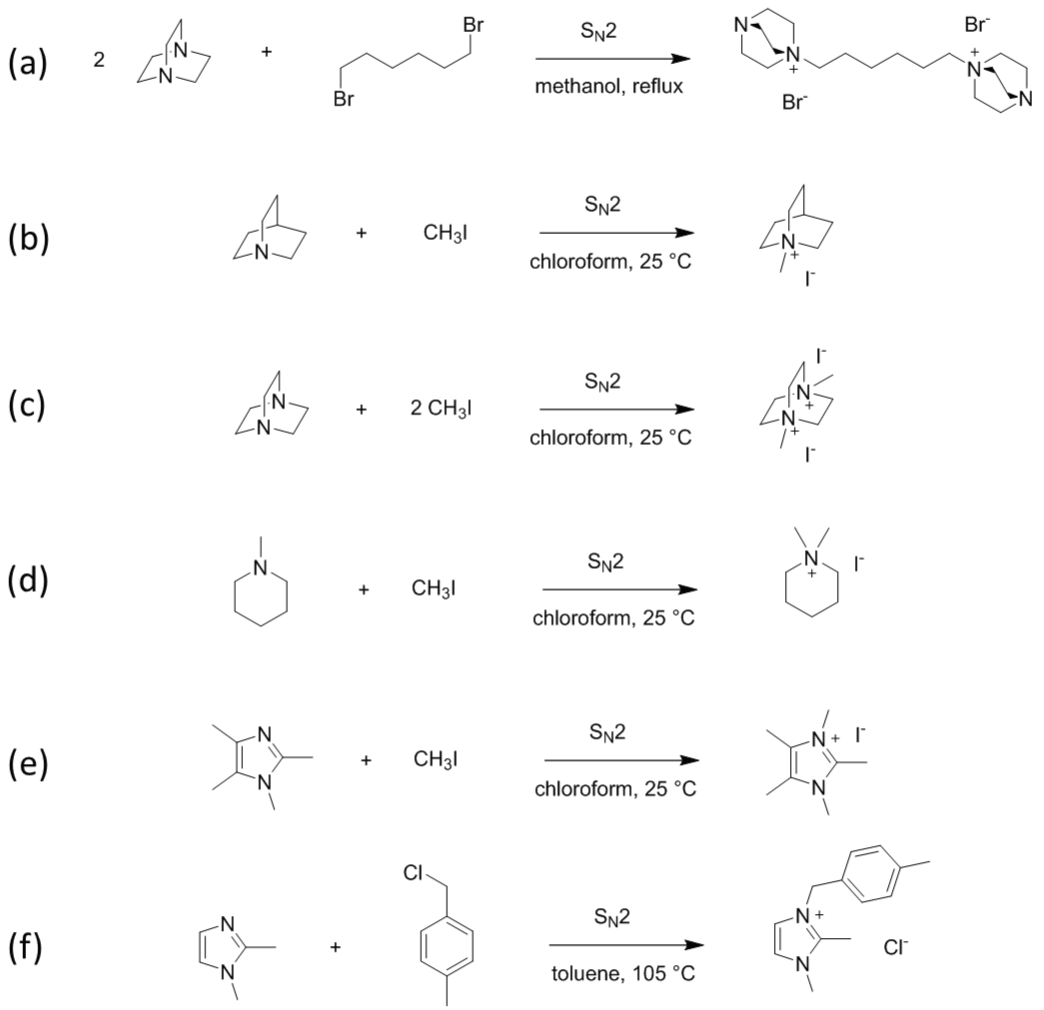

Figure 2.2. Reactions schemes for the OSDAs used to prepare the molecular sieve catalysts demonstrated in this work: (a) 1,1’-(hexane-1,6-diyl)bis(1,4-diazabicyclo[2.2.2]octanium), (b) N-methylquinuclidinium, (c) N,N’-dimethyl-1,4-diazabicyclo[2.2.2]octanium, (d) N,N-dimethylpiperidinium, (e) 1,2,3,4,5-pentamethylimidazolium, and (f) 1,2-dimethyl-3-(4-methylbenzyl)imidazolium.

Ion Exchange Synthesized halide-forms of OSDAs were ion-exchanged to their hydroxide forms. First, organic salts were dissolved in distilled water. And then, desired amounts of ion-exchange resin (Dowed^{TM} Monosphere^{TM} 550A OH, Dow Chemical) were added to the solution and stirred overnight. The mixing ratio was 1 mmol of OSDA : 3 mL of ion-exchange resin : 6 mL of distilled water. Used resin was separated by filtration and the same procedure was repeated using a new portion of ion-exchange resin. The final aqueous solutions of OSDAs as their quaternary ammonium hydroxide forms were concentrated to 100–200 mL using a rotary evaporator by evaporating excess water. The concentration of OSDA hydroxide was determined using an automatic titrator (Mettler Toledo Titrator DL22).

2.2.2. Synthesis of Microporous Materials

Materials All materials used for syntheses of microporous materials are used as-received without further purification steps. Moisture contents of silica or alumina sources were characterized on the basis of thermogravimetric analysis (TGA). For silica sources, colloidal silica (Ludox AS-series, Sigma-Aldrich), fumed silica (Cab-O-Sil®, ACROS), sodium silicate (Waterglass N®, 8.9 wt. % Na_2O, 28.7 wt. % SiO_2 in H_2O, PQ Corporation), and tetraethyl orthosilicate (TEOS, 99.9%, Alfa Aesar) were used. For alumina sources, aluminum hydroxide gel (Barcroft 250, 30.6 wt. % of moisture, SPI Pharma), pseudobohemite (Catapal B, 23.2 wt. % of moisture, VISTA), hydrated alumina (F2000, 33.8 wt. % of moisture, Reheis), sodium aluminate (37.9 wt. % Na_2O, 51.1 wt. % Al_2O_3, 11.0 wt. % H_2O, Alfa Aesar), and aluminum isopropoxide (98%, Sigma-Aldrich) were used. In some cases, zeolites Y were used as silica and alumina sources. Zeolyst CBV500 (Si/Al = 2.6, NH_4-form, 14.3 wt. % of moisture), CBV712 (Si/Al = 6, NH_4-form, wt. 15.1 % of moisture), and CBV720 (Si/Al = 15, H-form, wt. 8.8 % of moisture) were used. For phosphorus source, 85 wt. % orthophosphoric acid in water (Macron) was used. For cobalt sources, cobalt (II) sulfate hydrate (Sigma-Aldrich) and cobalt (II) acetate tetrahydrate (98%, Sigma-Aldrich) were used. For magnesium source, magnesium acetate tetrahydrate (98%, Sigma-Aldrich) was used. For hydroxide mineralizers, sodium hydroxide (pellets, EMD Milipore), potassium hydroxide solution (45 wt. % in water, Sigma-Aldrich), and cesium hydroxide solution (50 wt. % in water, Sigma-Aldrich) were used. For alkali metal sources, sodium nitrate (99.9%, Sigma-Aldrich) and potassium nitrate (99.9%, Sigma-Aldrich) were used.

The following OSDAs or organic additives were used as-received from the stated vendors: tetraethylammonium hydroxide (TEAOH, 35 wt. % in H_2O, Sigma-Aldrich), tetramethylammonium hydroxide (TMAOH, 25 wt. % in H_2O, Sigma-Aldrich), diethylamine (DEA, Sigma-Aldrich), morpholine (Sigma-Aldrich), cyclohexylamine (Sigma-Aldrich), diisopropylethylamine (DIPEA, Sigma-Aldrich), N,N,N-trimethyladamantylammonium hydroxide (AdaOH, 25 wt. % in H_2O, Sachem), 1,1,3,5-tetramethylpiperidinium hydroxide (TMPOH, 0.788 mmol g^{-1} in H_2O, Sachem), N,N,N',N'-tetramethylhexamethylenediamine (TMHD, 99%, Sigma-Aldrich), trimethylamine (TMA, 33 wt. % in ethanol, Fluka), tetra-n-butylammonium hydroxide (TBAOH, 55 wt. % in H_2O, Alfa Aesar), hexamethyleneimine (99%, Sigma-Aldrich), 1,4,7,10,13,16-hexaoxacyclooctadecane (18-crown-6 ether, 99%, Sigma-Aldrich), 1,4,8,11-tetraazacyclotetradecane (Cyclam, 98%, Sigma-Aldrich), 4,7,13,16,21,24-hexaoxa-1,10-diazabicyclo[8.8.8]hexacosane (Kryptofix® 222 or just K222, 98%, Sigma-Aldrich), and cetyltrimethylammonium bromide (CTAB, Sigma-Aldrich).

The preparation protocols of the following OSDAs were provided above: 1,1'-(hexane-1,6-diyl)bis(1,4-diazabicyclo[2.2.2]octanium) dihydroxide (C_6-diDABCO-OH_2), N-methylquinuclidinium hydroxide ($MQuin^+OH^-$), N,N'-dimethyl-1,4-diazabicyclo[2.2.2]octanium dihydroxide ($DMDABCO^{2+}(OH^-)_2$), N,N-dimethylpiperidinium hydroxide (DMP^+OH^-) 1,2,3,4,5-pentamethylimidazolium hydroxide (PMI^+OH^-), 1,2-dimethyl-3-(4-methylbenzyl)imidazolium hydroxide ($12DM34MBI^+OH^-$).

General Procedures All zeolites and $AlPO_4$-based molecular sieves used in this work were prepared on the basis of the general procedures described here unless otherwise mentioned.

For zeolites, firstly, alumina source material was dissolved in alkali and/or OSDA hydroxide solution and stirred until the mixture became clear or translucent. And then, silicon source was added and digested under stirring for extra 24 hours.

For $AlPO_4$-based molecular sieves, alumina source was mixed with twofold weight of water and stirred for 2 hours. And using a separate polytetrafluoroethylene (PTFE) beaker, a desired amount of concentrated phosphoric acid was mixed with the same weight of water and transferred to the alumina-water mixtures slowly. This aluminophosphate mixture was stirred for 3 hours. And then, silica or other metal sources and the rest of the desired amount of water (if any) were added to the gel. OSDA was added to the mixture 30 min after the silica addition. The final gel was stirred for extra 24 hours. Excess water was evaporated using an air flow if necessary after that.

Gel having the desired compositions were transferred to a 23-mL PTFE liner for Parr autoclave, and sealed tightly. Crystallizations were performed at desired temperatures in rotary or static convection ovens. Aliquots of the batch were taken periodically, and PXRD patterns of them were acquired to monitor the crystallization progress.

$AlPO_4$-based Materials Syntheses The cage structures of $AlPO_4$-based molecular sieves used in this work and the structures of OSDAs used to synthesize the corresponding molecular sieves were demonstrated in Figure 2.3.

SAPO-34 was prepared from TEAOH.[64] The molar composition of the gel was 1 Al_2O_3 : 1 P_2O_5 : 0.075 SiO_2 : 3 TEAOH : 50 H_2O. Catapal B alumina and Ludox HS-40 silica sol were used as the aluminum and silicon sources, respectively. The crystallization was performed at 200 °C in a static oven for 24 hours.

CoAPO-34 and MgAPO-34 were synthesized by using morpholine as the OSDA.[20-21] The gel composition was x Al_2O_3 : 1 P_2O_5 : y MO (M = Co, Mg) : 2.7 Morpholine : 60 H_2O. For (x,y), (0.8, 0.4) and (0.7, 0.6) were tried. The aluminum, cobalt, and magnesium sources used here were Catapal B alumina, cobalt (II) sulfate hydrate, and magnesium acetate tetrahydrate, respectively. The crystallization was performed at 185 °C in a rotating oven for 72 hours.

SAPO-56 was synthesized using TMHA as the OSDA.[65] The gel composition was 0.8 Al_2O_3 : 1.0 P_2O_5 : 0.3–0.6 SiO_2 : 2 TMHA : 40 H_2O. Catapal B alumina and Cab-O-Sil fumed silica were used as the aluminum and silicon sources, respectively. The crystallization was performed at 200 °C in a static oven for 96 hours.

STA-18 was synthesized using C_6-diDABCO-Br_2 and TMA as the co-OSDAs.[58] The gel composition was 1.0 $Al(OH)_3$: 0.7 H_3PO_4 : 0.3 SiO_2 : 0.08–0.10 C_6-diDABCO-Br_2 : 0.13 TMA : 0.28 TBAOH : 40 H_2O. Aluminum hydroxide hydrogel and Cab-O-Sil fumed silica were used as the aluminum and silicon sources, respectively. The crystallization was performed at 190 °C in a rotating oven for 7 days.

SAPO-35 was synthesized using hexamethyleneimine as the OSDA with a gel composition: 1.0 Al_2O_3 : 1.0 P_2O_5 : 0.3–0.6 SiO_2 : 1.5 hexamethyleneimine : 55 H_2O.[39] Catapal B alumina and Cab-O-Sil fumed silica were used as the aluminum and silicon sources, respectively. The crystallization was performed at 200 °C in a static oven for 24 hours. SAPO-16 (AST) was observed as the major impurity phase, but it could be separated from SAPO-35 by repeated steps of fractional centrifugation at 500 rpm.

SAPO-18 was prepared from TMPOH.[66] The gel composition was 1 Al_2O_3 : 0.8 P_2O_5 : 0.172 SiO_2 : 1 TMPOH : 19.2 H_2O. The aluminum and silicon sources were Catapal B (VISTA) alumina and Ludox AS-40 silica sol (Sigma-Aldrich). The crystallization was performed at 190 °C in a rotating oven for 2 days.

CoAPO-18 and MgAPO-18 were prepared from the same diisopropylethylamine (DIPEA) OSDA with a gel composition of 1 Al_2O_3 : 1 P_2O_5 : 0.08 MO (M = Co, Mg) : 1.7 DIPEA : 50 H_2O.[67] The crystallization was performed at 160 °C in a rotating oven for 8–11 days.

STA-7 was synthesized using Cyclam as the OSDA.[42] The gel composition was 1.0 $Al(OH)_3$: 0.6–0.8 H_3PO_4 : 0.2–0.4 SiO_2 : 0.108 Cyclam : 40 H_2O. The aluminum and silicon sources were aluminum hydroxide dry-gel (Barcroft 250, SPI Pharma) and fumed silica. The crystallization was performed at 190 °C in a rotating oven for 72 hours. In some cases, white fluffy impurity was observed, and required extra purification steps. The desired STA-7 product was slightly yellowish and denser than the white impurity phase. The purification was performed using the fractional centrifugation at 500 rpm in distilled water. The top white phase was removed from the mixture by repeated centrifugation.

DNL-6 was synthesized using DEA and CTAB.[68] The gel composition was 1.0 $Al(OH)_3$: 0.8 H_3PO_4 : 0.2 SiO_2 : 1 DEA : 0.10–0.15 CTAB : 50 H_2O. The aluminum and silicon sources were aluminum isopropoxide and TEOS. The hydrolysis alcohol products (i.e., ethanol and isopropanol) were removed by heating the gels at 80 °C. The crystallization was performed at 160 °C in a rotating oven for 48 hours.

SAPO-42 and STA-14 were synthesized using K222 and TEAOH as the OSDAs.[42] The gel composition was 1.0 $Al(OH)_3$: 0.8 H_3PO_4 : 0.2 SiO_2 : 0.108 K222 : 0.108x TEAOH : 40 H_2O where $x = 0$–6. When $x < 2$, SAPO-42 was obtained, and when $x > 5$, STA-14 was obtained. This implies that TEA$^+$ cations can structure-direct the *pau* small cages in this system. The crystallization was performed at 190 °C in a rotating oven for 48 hours.

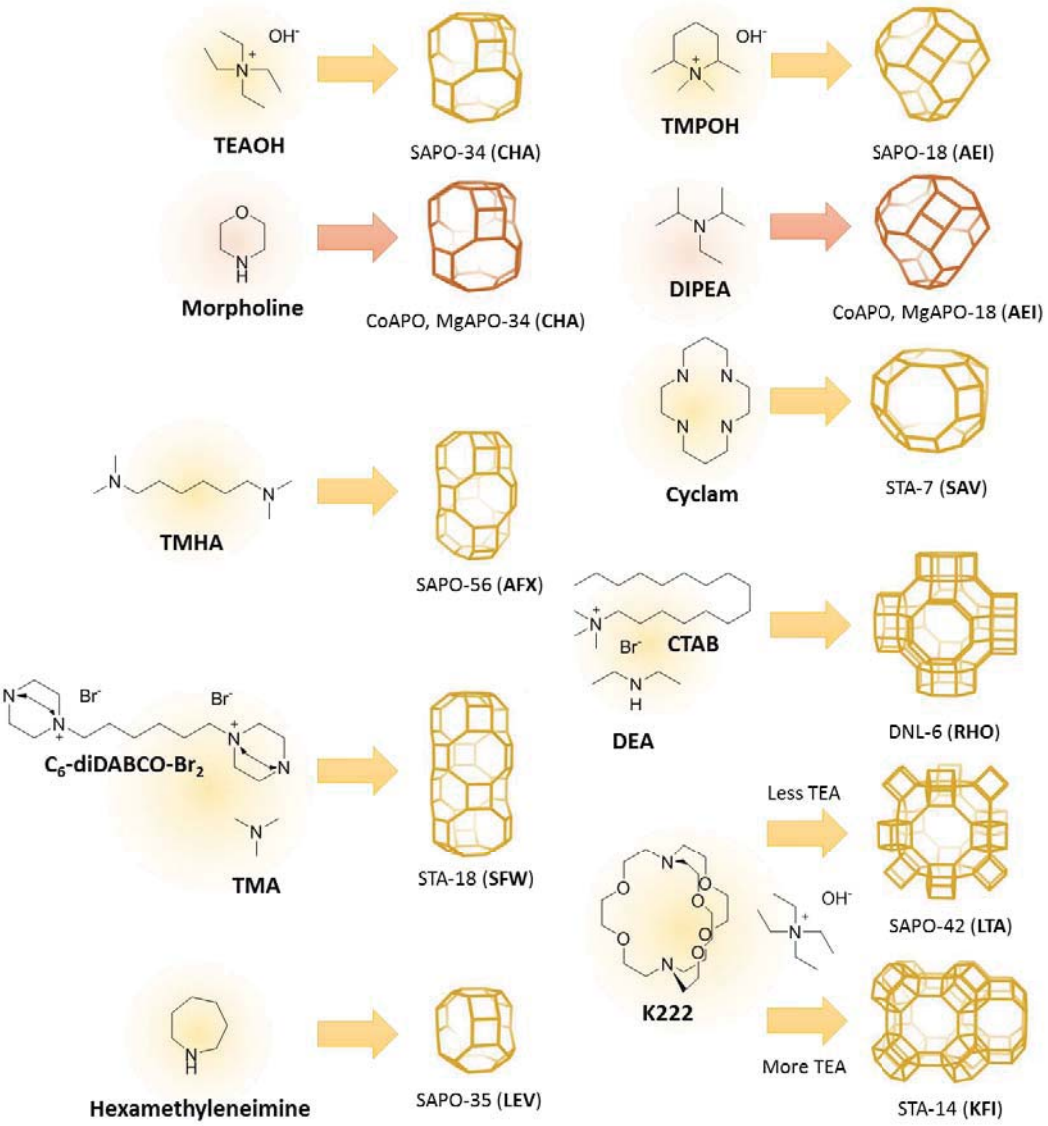

Figure 2.3. OSDAs and cage structures of the corresponding resultant $AlPO_4$-based molecular sieves.

Zeolites Syntheses The cage structures of zeolites used in this work and the structures of OSDAs used to synthesize the corresponding zeolites were demonstrated in Figure 2.4.

SSZ-13 was prepared using AdaOH as the OSDA.[18] Desired amounts of AdaOH solution, sodium hydroxide and distilled water were mixed. A desired amount of sodium aluminate was dissolved in the mixture and stirred for 1 hour. And then, a desired amount of fumed silica was added. The gel composition was 1 SiO_2 : 0.017 Al_2O_3 : 0.20 AdaOH : 0.20 NaOH : 44 H_2O. The mixture was stirred for 24 hours before starting the crystallization. The crystallization was performed in a 160 °C rotating oven for 6–8 days.

SSZ-39 was prepared by converting commercial Y zeolite using a one-to-one-ratio cis/trans mixture of N,N,3,5-tetramethylpiperidinium hydroxide (TMPOH) as the OSDA. The synthesis was performed without use of sodium hydroxide, modified from ref [69]. Desired amounts of fumed silica, OSDA solution, and distilled water were mixed in a PTFE liner and homogenized by stirring. After that, a desired amount of Zeolyst CBV500 was dispersed in the mixture. Further aging steps at room temperature did not influence the results. The final gel composition was 1 SiO_2 : 0.067 Al : 0.706 TMPOH : 20.38 H_2O. The crystallization was performed in a 140 °C rotating oven for 28 days.

The LEV zeolites used in this work were synthesized using two methods with the following OSDAs: MQuinOH[59] and $DMDABCO(OH)_2$.[61] The LEV zeolite synthesized using MQuinOH as the OSDA is known as Nu-3 (or SSZ-17), and has high silica elemental compositions (Si/Al > 10). Desired amounts of MQuinOH solution, sodium hydroxide and distilled water were mixed. A desired amount of Reheis F2000 hydrated alumina was dispersed in the mixture and stirred for 1 hour. Then, colloidal silica Ludox AS-40 was added dropwise. The gel composition was 1 SiO_2 : 0.024 Al_2O_3 : 0.199 MQuinOH : 0.187 NaOH : 40.11 H_2O. The mixture was stirred for 24 hours before starting the crystallization. The crystallization was performed in a 175 °C rotating oven for 6 days.

A lower-silica LEV zeolite was prepared using DMDABCO(OH)$_2$ as the OSDA. Desired amounts of 20% sodium hydroxide solution, sodium silicate, DMDABCO(OH)$_2$ solution, and distilled water were mixed in a PTFE liner and homogenized by stirring. Next, a desired amount of Zeolyst CBV720 was dispersed in the mixture. The mixture was stirred for 1 day. A desired portion of water was evaporated using flowing air. The final gel composition was 1 SiO$_2$: 0.0147 Al : 0.178 DMDABCO(OH)$_2$: 0.580 NaOH : 9.43 H$_2$O. The crystallization was performed in a 150 °C rotating oven for 3 days.

SSZ-98 was prepared by converting commercial Y zeolite using N,N-dimethylpiperidinium hydroxide (DMPOH) as the OSDA.[60] Desired amounts of DMPOH solution, potassium hydroxide solution and water was mixed in a PTFE liner and stirred. Next, a desired amount of Zeolyst CBV720 was dispersed in the mixture. The mixture was sealed and transferred to a 150 °C static oven. The final gel composition was 1 SiO$_2$: 0.033 Al$_2$O$_3$: 0.267 DMPOH : 0.497 KOH : 38.840 H$_2$O. The crystallization was performed for 3 days.

Zeolite RTH was prepared using PMIOH as the OSDA.[48] Desired amounts of TEOS and aluminum isopropoxide were hydrolyzed in a mixture of PMIOH solution by stirring at room temperature for 24 hours. Next, excess amounts of water and alcohol species formed as the results of hydrolysis were evaporated under flowing air. Desired amount of hydrogen fluoride (HF, 45 wt. % in H$_2$O, Sigma-Aldrich) was added dropwise to the gel. (*Caution: Hydrogen fluoride is a dangerous substance that can cause fatal burns and irreversible damages to human skin, tissue, and bone. It must be handled with appropriate PPE including a lab coat, a respirator, a full-face shield, an acid-apron, a pair of long-sleeve nitrile gloves, etc. with a proper ventilation in a fume hood.*) The viscous transparent gel became powdery as a result of the addition of HF. The resultant fluoride gel was further dried in a fume hood for 1–2 days. A desired amount of distilled water was added to achieve the desired gel composition. The final gel composition was 0.95 SiO$_2$: 0.05 Al : 0.5 PMIOH : 0.50 HF : 7.0

H_2O. The crystallization was performed in a 160 °C rotating oven for 2 weeks. Decreasing aluminum contents in gels (below Si/Al = 50) resulted in the formation of high-silica STW impurities.

High-silica LTA zeolite was prepared using $12DM34MBI^+OH^-$ and TMAOH as the co-OSDAs in fluoride media.[62] Desired amounts of TEOS and aluminum isopropoxide were hydrolyzed in a mixture of $12DM34MBI^+OH^-$ and TMAOH solution by stirring at room temperature for 24 hours. Next, excess amounts of water and alcohol species formed as the results of hydrolysis were evaporated under flowing air. Desired amount of hydrogen fluoride (HF, 45 wt. % in H_2O, Sigma-Aldrich) was added dropwise to the gel. (*Caution: Hydrogen fluoride is a dangerous substance that can cause fatal burns and irreversible damages to human skin, tissue, and bone. It must be handled with appropriate PPE including a lab coat, a respirator, a full-face shield, an acid-apron, a pair of long-sleeve nitrile gloves, etc. with a proper ventilation in a fume hood.*) The viscous transparent gel became powdery as a result of the addition of HF. The resultant fluoride gel was further dried in a fume hood for 1–2 days. A desired amount of distilled water was added to achieve the desired gel composition. Pure-silica LTA was added as the seed lastly. The final gel composition was 0.95–0.99 SiO_2 : 0.013–0.048 Al : 0.45 $12DM34MBI^+OH^-$: 0.05 TMAOH : 0.50 HF : 5.0 H_2O. The crystallization was performed in a 125 °C static oven for 1–3 weeks. Increasing the aluminum contents in gels required longer crystallization times.

Zeolite Rho was synthesized using 18-crown-6 ether as the OSDA as Chatelain et al. have described.[70] Ludox HS-40 and sodium aluminate were used as the silica and alumina sources, respectively. The gel composition was 1 SiO_2 : 0.1 Al_2O_3 : 0.130 Na_2O : 0.030 Cs_2O : 0.050 18-crown-6 : 10.0 H_2O. The crystallization was performed in a 110 °C static oven for 2–8 days.

Zeolite KFI was synthesized without OSDAs.[71] Zeolyst CBV712 was used as the sole silica and alumina source. Desired amounts of sodium hydroxide, sodium nitrate, and potassium nitrate were dissolved in distilled water. After that, a desired amount zeolite Y was dispersed in the solution. The final gel composition was 1 SiO_2 : 0.0833 Al_2O_3 : 3.3 Na^+ : 7.0 K^+ : 0.56 OH^- : 9.74 NO_3^- : 117 H_2O. The crystallization was performed in a 140 °C static oven for 3 days. The same procedure was repeated for 3 times by wet-seeding the next batches with a portion of the previous batch used to enhance the crystallinity.

UZM-5 zeolite was prepared based on the charge density mismatch (CDM) synthesis strategy.[43] Colloidal silica AS-40 and aluminum isopropoxide were used as the silica and alumina sources, respectively. The final gel composition was 1 SiO_2 : 0.063 Al_2O_3 : 1.0 TEAOH : 0.125 TMAOH : 29.438 H_2O. The crystallization was performed in a 150 °C rotating oven for 10 days.

Other zeolites, high and low silica SSZ-16,[72] SSZ-52,[73] SSZ-105,[74] SSZ-99,[75] SSZ-104,[76] SSZ-27,[77] SSZ-28,[78] and ITQ-3-type zeolite,[79] were thankfully provided by Dr. Stacey I. Zones, Dr. Dan Xie, and Dr. Tracy M. Davis from Chevron Energy Technology Company. The synthesis protocols of these zeolites are disclosed in the cited patents and articles.

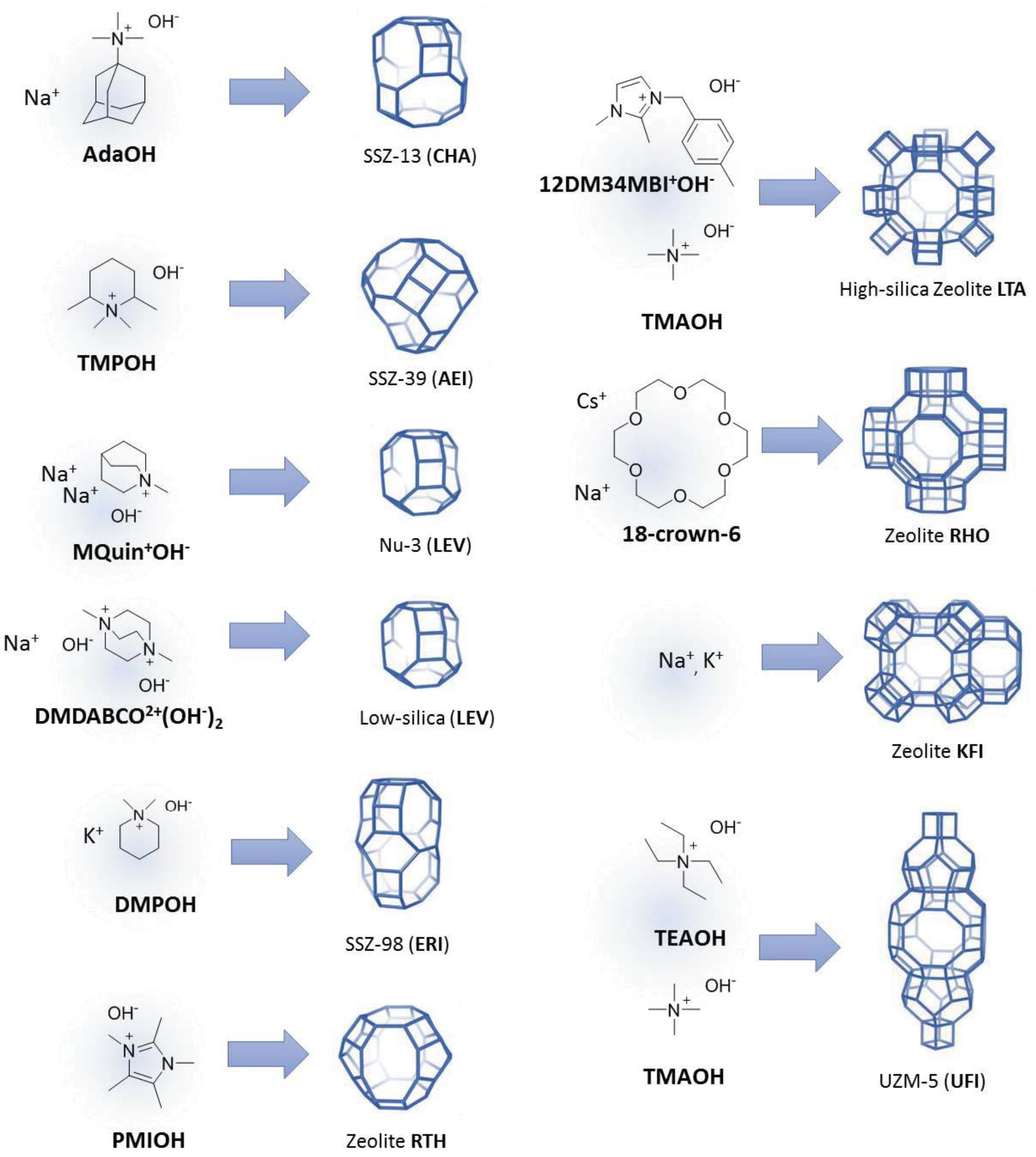

Figure 2.4. OSDAs and cage structures of the corresponding resultant zeolites.

2.2.3. Characterization of Microporous Materials

To identify the product catalysts, powder X-ray diffraction profiles were collected using a Rigaku Miniflex II benchtop diffractometer with Cu Kα radiation (λ = 1.54184 Å).

Morphology and elemental composition of obtained molecular sieves were characterized using a field-emission scanning electron microscope (FE-SEM, ZEISS 1550VP) and an energy dispersive spectrometer (EDS, Oxford X-Max SDD).

2.2.4. MTO Reaction

All catalysts demonstrated in this work were tested in their NH_4-forms or H-forms, if necessary, by repeated cycles of ion-exchange with 1 M ammonium nitrate solution. (1 g solid : 100 mL solution, 85 °C, 2–5 times until alkali elements are invisible in EDS spectra)

For every reaction, ca. 200 mg of catalyst was pelletized to be 0.18–0.60 mm in granule size. A pelletized catalyst bed was placed in a steel tubular reactor (0.25' in diameter and 6" in length) between a pair of glass wool blocks. The bed was activated under an air flow at 580 °C for 12 hours. The dry weight of catalyst was estimated on the basis of a TGA profile which was separately acquired. (TGA: PerkinElmer STA6000) The reaction was conducted at strictly 400 °C. The methanol feed was diluted to be 10% in a carrier gas flow (95% He and 5% internal standard Ar, flow rate: 30 mL min^{-1}). Based on the dry weight of the catalyst bed, weight-hourly space volume of methanol (WHSV) was adjusted to be 1.3 h^{-1}. The product distributions were quantified using a GC-MS system (GC: Agilent GC 6890N, MS: Agilent MS 5973N). The reaction outlet flow was sampled every 16 min.

The amount of hydrocarbon products formed over the catalysts were evaluated by calculating the selectivities from the resultant GC-chromatograms. All selectivity values in this work were calculated on the carbon-number basis. The selectivity was defined as follows:

$$\text{Selectivity}(t = \text{TOS}) = \frac{\text{NC} \times n_{\text{product}}(t = \text{TOS})}{n_{\text{MeOH}}(t = 0) - n_{\text{MeOH}}(t = \text{TOS})}$$

where NC, $n_{product}$, and n_{MeOH} are the number of carbon atoms in a single hydrocarbon molecule, the molar flow rate of the hydrocarbon, and the molar flow rate of the methanol, respectively. The product distributions were calculated by averaging selectivities in the ranges of 98 to 100% methanol conversion.

2.3. Result and Discussion

2.3.1. Materials Characterization

In this section, PXRD patterns and SEM micrographs of obtained molecular sieves were provided. Also, elemental compositions of them are mentioned in the text. The Al contents of zeolites were expressed in Si/Al molar ratios. For $AlPO_4$-based materials, M/T ratios (M = Si, Co, Mg; T = M+Al+P) were offered.

Four CHA-type molecular sieves (SSZ-13, SAPO-34, CoAPO-34, and MgAPO-34) were prepared for the MTO reaction study. PXRD patterns of the resultant materials are shown in Figures 2.5(a-d). All four molecular sieves showed PXRD profiles consistent with the CHA-topology and the previously reported results.[20-21, 64] Minor differences in intensities and positions of the diffraction peaks are probably due to the difference among their elemental compositions. Figures 2.5(e-h) are the SEM images of these molecular sieves. These CHA-type molecular sieves had polycrystalline rhombohedral-to-cubic morphologies in common, and relatively large sizes (20–30 μm) except for SAPO-34. SAPO-34 showed a higher heteroatom concentration (Si/T = 0.123) than the other two MAPO-34s (Co/T = 0.022 for CoAPO-34, and Mg/T = 0.015).

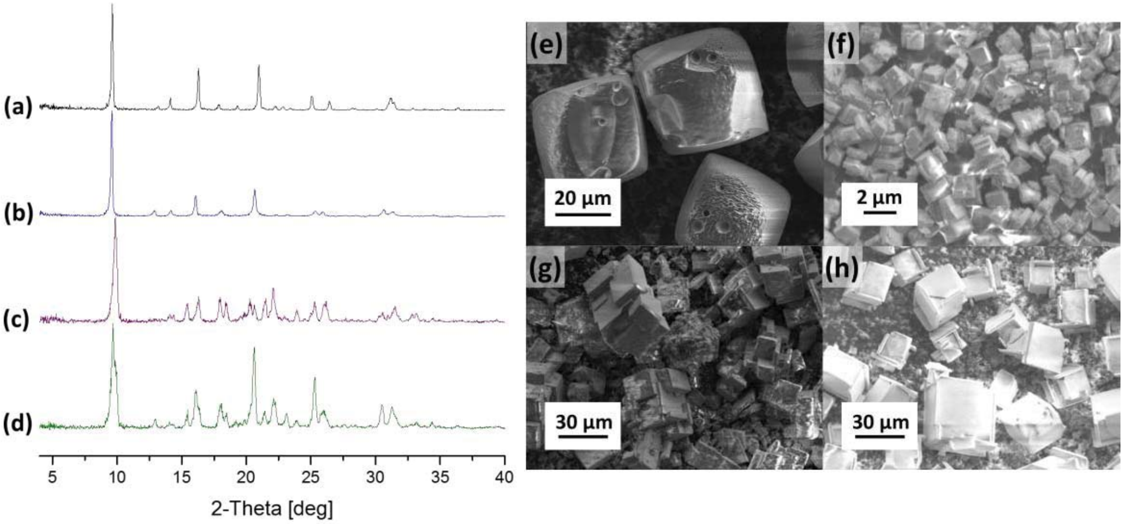

Figure 2.5. PXRD profiles of as-prepared (a) SSZ-13, (b) SAPO-34, (c) CoAPO-34, and (d) MgAPO-34. SEM images of (e) SSZ-13, (f) SAPO-34, (g) CoAPO-34, and (h) MgAPO-34.

SSZ-99 and SSZ-104 are CHA/GME-intergrowth zeolites.[75-76] Since both CHA and GME belong to the ABC-6-type frameworks, the two topologies can coexist in one crystal by stacking faults of the d6r units along the *c*-axis. Figures 2.6(a, b) show the PXRD profiles of SSZ-99 and SSZ-104. The presence of the diffraction at 2θ = ca. 7.5° and generally broad shapes of peaks indicates that these are CHA/GME intergrowth zeolites. The crystal sizes were smaller than pure CHA-type molecular sieves shown above, and the Si/Al ratios of these zeolites were relatively low (Si/Al = 3.7 for SSZ-99, and 3.6 for SSZ-104).

SSZ-105 is another intergrowth zeolite of ERI and LEV.[74] Similarly to the CHA-GME pair mentioned above, both ERI and LEV also belong to the ABC-6 family, but these two frameworks have single-6-ring (*s*6*r*) layers unlike CHA and GME which are completely composed of *d*6*r* units. The PXRD profile of SSZ-105 (Figure 2.6(f)) showed broad peaks related to both LEV and ERI, and it was reported that this diffraction pattern is consistent with the DIFFaX-simulated patterns for ERI-LEV intergrowth crystals.[74]

SSZ-27 is a novel small-pore/cage zeolite having one-dimensional channel system.[77] It has a unique heart-shaped cage structure (Figure 2.6(h)) which resembles that of ITQ-55 that showed an excellent separation performance for ethylene-ethane mixtures,[80] but there is a difference in cage-connectivity between SSZ-27 and ITQ-55. The provided SSZ-27 had a Si/Al ratio of 14.7.

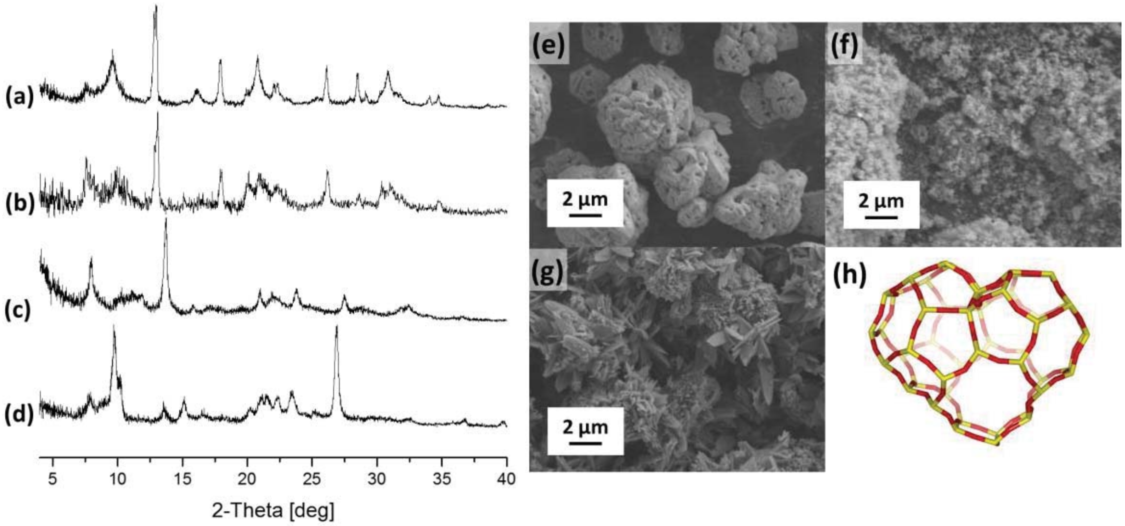

Figure 2.6. PXRD profiles of (a) SSZ-99, (b) SSZ-104, (c) SSZ-105, and (d) SSZ-27. SEM images of (e) SSZ-99, (f) SSZ-105, and (g) SSZ-27.

AFX and SFW are another two topologies belonging to the ABC-6-type frameworks. For AFX-type molecular sieves, two SSZ-16 zeolites and SAPO-56 were prepared. The two SSZ-16 had similar hexagonal morphologies, and the high-silica sample had a bigger crystal size (2–5 µm) than the low-silica sample (ca. 1 µm) (Figure 2.7(e–f)). The Si/Al ratios of the two SSZ-16 were 14.7 and 6.2, respectively. SAPO-56 had a hexagonal disc-like morphology and a Si/T ratio of 0.137. The SFW topology was also realized as both zeolite and SAPO: SSZ-52[73] and STA-18.[58] The crystal size of SSZ-52 was ca. 1 μm, and its Si/Al ratio was 6.1. STA-18 had a polycrystalline hexagonal plate-like morphology, and the Si/T ratio was 0.176.

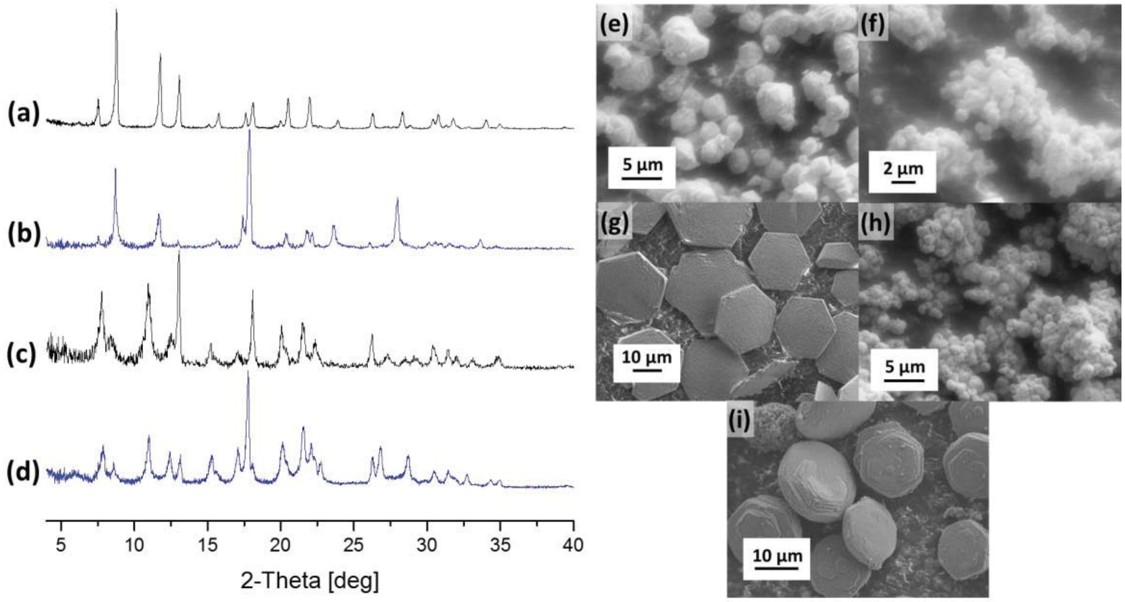

Figure 2.7. PXRD profiles of as-prepared (a) high-silica SSZ-16, (b) SAPO-56, (c) SSZ-52, and (d) STA-18. SEM images of (e) high-silica SSZ-16, (f) low-silica SSZ-16, (g) SAPO-56, (h) SSZ-52, and (i) STA-18.

For the LEV topology, two zeolites from two different OSDAs—MQuin$^+$ and DMDABCO^{2+}—and SAPO-35 were prepared. In this work, the LEV zeolite synthesized using MQuin$^+$ is called Nu-3, and the other is called DMDABCO-LEV. The crystal sizes of both Nu-3 and DMDABCO-LEV were ca. 1 μm. (Figures 2.8(e–f)) The Si/Al ratios of Nu-3 and DMDABCO-LEV were 17.7 and 8.3, respectively. Contrary to the LEV-type zeolite counterparts, SAPO-35 had a very large (ca. 20 μm) crystal size, and its Si/T ratio was 0.120. The ERI topology was realized as zeolite SSZ-98 which is recently discovered. Crystal size and Si/Al ratio of the synthesized SSZ-98 were 1–2 μm and 6.0, respectively.

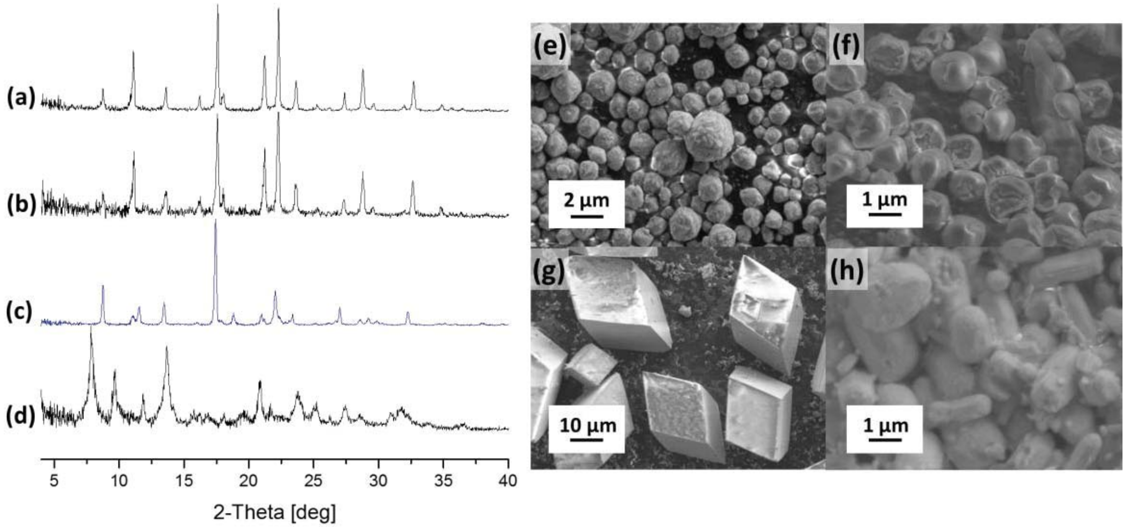

Figure 2.8. PXRD profiles of (a) Nu-3, (b) DMDABCO-LEV, (c) SAPO-35, and (d) SSZ-98. SEM images of (e) Nu-3, (f) DMDABCO-LEV, (g) SAPO-35, and (h) SSZ-98.

AEI is the other topology that was prepared as four different elemental compositions other than CHA. SSZ-39, SAPO-18, CoAPO-18, and MgAPO-18 were prepared and their PXRD patterns and SEM images are shown in Figure 2.9. Generally, the AEI-type molecular sieves had much smaller crystal sizes (< 1 μm) than the CHA-type microporous materials (*vide supra*). The Si/Al ratio of SSZ-39 synthesized without alkali cation was 10.0, and heteroatom molar ratios of $AlPO_4$-18-based materials were 0.062, 0.073, and 0.031 for SAPO-, CoAPO-, and MgAPO-18, respectively.

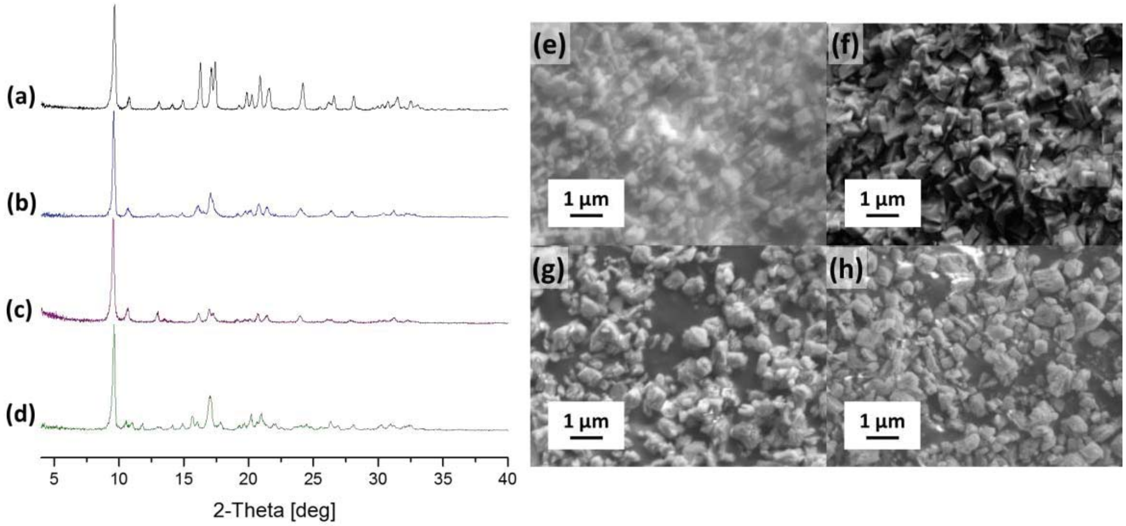

Figure 2.9. PXRD profiles of (a) SSZ-39, (b) SAPO-18, (c) CoAPO-18, and (d) MgAPO-18. SEM images of (e) SSZ-39, (f) SAPO-18, (g) CoAPO-18, and (h) MgAPO-18.

Figure 2.10. shows PXRD patterns and SEM images of several other small-pore zeolites and $AlPO_4$-based molecular sieves. Since the frameworks DDR, RTH, and ITE have building units composed of odd numbers of T-atoms (e.g., 5-membered ring), $AlPO_4$-based molecular sieves having these topologies cannot exist in principle. Also, zeolites having SAV topology are not discovered yet. Zeolite DDR (SSZ-28, Si/Al = 18.8), RTH (Si/Al = 13.2), and ITE (Si/Al = 18.1) tested in this work had moderately high Si/Al ratios and different morphologies and crystal sizes (Figure 2.10(e–g)). For SAV, Two STA-7 samples were prepared having different Si contents (Si/T = 0.133 and 0.185). They are denoted STA-7(1) (Si/T = 0.133) and STA-7(2) (Si/T = 0.185), respectively. Their crystal morphologies reflected their tetrahedral unit cell symmetries. SEM image of STA-7(1) is shown in Figure 2.10(h). (STA-7(2) is now shown here.)

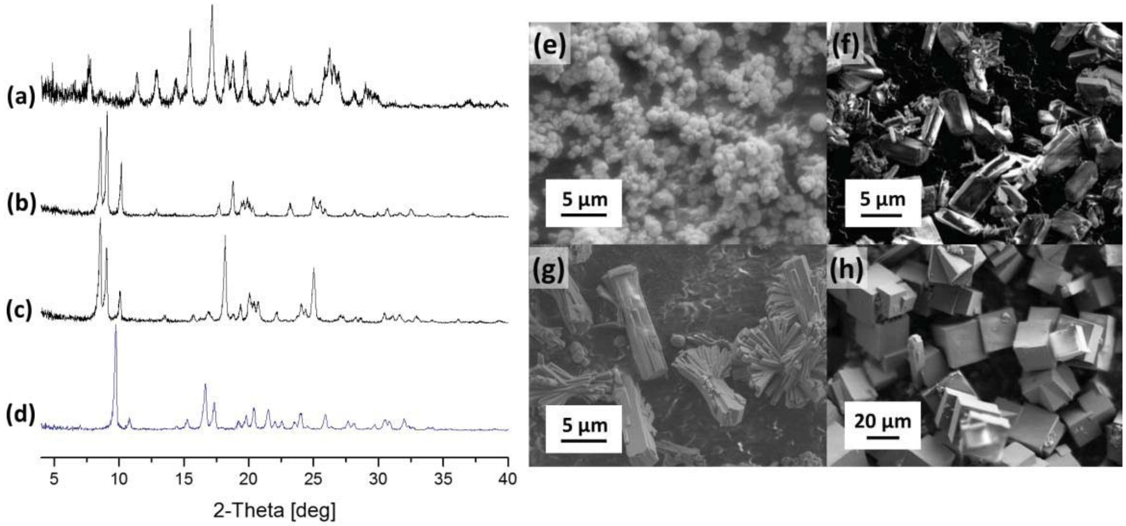

Figure 2.10. PXRD profiles of (a) SSZ-28, (b) Zeolite RTH, (c) Zeolite ITE, and (d) STA-7. SEM images of (e) SSZ-28, (f) Zeolite RTH, (g) Zeolite ITE, and (h) STA-7(1).

Four following topologies having LTA-cages were also prepared as zeolites and SAPO-based materials: LTA, RHO, KFI, and UFI. PXRD patterns and SEM micrographs of these molecular sieves are displayed in Figure 2.11. Similarly to DDR, RTH, and ITE mentioned above, UFI has building units (e.g. *rth* composite building unit) that is composed of odd number of T-atoms. So the topology UFI was realized as its only one known zeolite form, UZM-5. The other three LTA-cage-possessing frameworks are prepared both as zeolites and SAPOs.

High silica LTA zeolite and SAPO-42 represent the LTA framework here. They showed cubic or truncated-cubic topology, and their Si/Al ratio and Si/T ratio were 28.8 and 0.150, respectively. Zeolite RHO and SAPO-RHO (DNL-6) also showed truncated cubic crystal shapes. Zeolite RHO had a relatively low Si/Al ratio, 5.4. DNL-6 demonstrated a moderate Si content (Si/T = 0.140). Also Zeolite KFI had a low Si/Al ratio of 4.0, probably due to the absence of bulky OSDA cations in its synthesis gel. A SAPO-version of KFI is STA-14, and it had a moderate Si/T ratio, 0.113. STA-14 and SAPO-42 could be synthesized from the same dual-OSDA system of K222 and TEAOH. STA-14 was the preferred product when TEAOH concentration in gels was high (TEA$^+$/K222 molar ratio > 5).

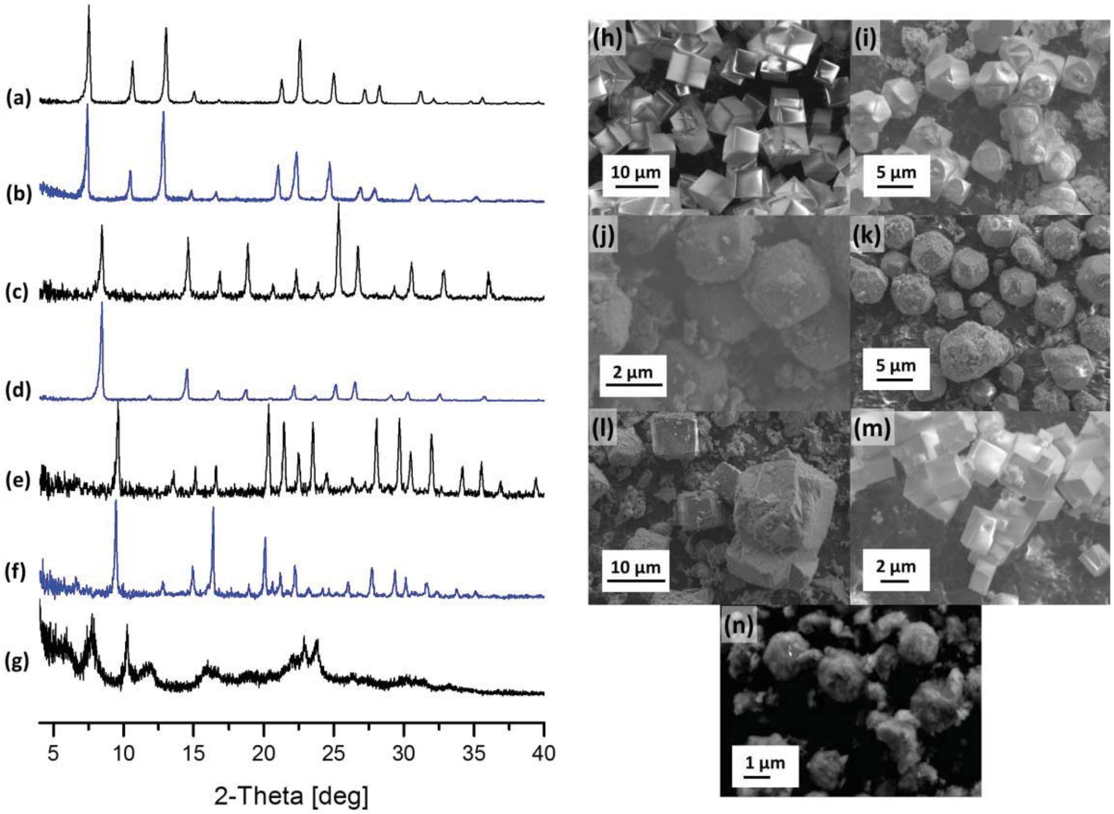

Figure 2.11. PXRD profiles of (a) Zeolite LTA, (b) SAPO-42, (c) Zeolite RHO, (d) DNL-6, (e) Zeolite KFI, (f) STA-14, and (g) UZM-5. SEM images of (h) Zeolite LTA, (i) SAPO-42, (j) Zeolite RHO, (k) DNL-6, (l) Zeolite KFI, (m) STA-14, and (n) UZM-5.

2.3.2. MTO Reaction Results

In this section, the MTO time-of-stream (TOS) selectivity charts of catalysts introduced in the previous section are exhibited. The extents of reactions are monitored by evaluating selectivities of light olefins (ethylene, propylene, and butylenes), alkanes (ethane, propane, and butanes), dimethyl ether (DME) and methanol conversion based on gas chromatograms taken every 16 min. All reactions are conducted at 400 °C with a methanol flow of WHSV = 1.3 h^{-1}.

The CHA-type molecular sieves are the most extensively studied class of catalysts due to their high selectivities toward light olefins (ca. 85–90%) and excellent thermal stability and lifetime. All CHA-type catalysts shown here exhibited very high ethylene and propylene selectivities. SAPO-34, which is the catalyst being used in commercial processes,[13] showed the longest lifetime (85% MeOH conversion at 259 min) among all four CHA-type catalysts. However, the lifetime cannot be the unique strength of SAPO-34 because it can be modified by controlling crystal sizes or nature of acid-sites.[64, 81-83] Most importantly, since these catalysts are continuously regenerated by the co-operating regeneration unit in actual commercial MTO fluidized reactors,[13, 84] the importance of lifetime performances of catalysts evaluated in an in-lab microscale fixed-bed reactor should not be overestimated.

SSZ-13 showed an ‘ethylene-propylene selectivity crossing’ behavior which has been observed in many previous reports.[64, 85] Propylene was formed with a relatively constant selectivity, while the ethylene selectivity continuously increased from initial 29.3% to 46.3% at the onset of catalyst deactivation. This behavior different to that of SAPO-34 is known to be due to strong acidity of zeolites stronger than that of SAPOs.[86] Deimund et al. experimentally showed that this evolution of olefin selectivity significantly depends on the acid-site density of SSZ-13, and suggested that MTO behavior of SSZ-13 would eventually resemble that of SAPO-34 by increasing Si/Al ratio of SSZ-13.[64] However, regardless of the acid-site density of the two types of materials, their ethylene-to-propylene selectivity ratios were close to unity.

MTO-catalytic performances of pure CoAPO-34 or MgAPO-34 have been very rare in literature up to date. CoAPO-34 and MgAPO-34 also showed very high overall light olefin selectivities (80–85%), but their lifetimes were shorter than SAPO-34, probably due to their large crystal sizes. Their olefin product distribution were also similar to that of SSZ-13. Cobalt (II) and magnesium can also form Brønsted acid sites within CHA-type $AlPO_4$ frameworks by replacing aluminum with moderate acidity.[20-21] According to the previous reports, both CoAPO-34 and MgAPO-34 have weaker structural Brønsted acidities than SAPO-34; on the basis of ammonia (NH_3)-temperature programmed desorption (TPD), both Co- and Mg-substituted $AlPO_4$-CHA molecular sieves showed maximum ammonia desorption at approximately 350 °C, much lower than ca. 450 °C shown by SAPO-34.[20-21] Ashtekar et al. reported that CoAPO-34 was transformed to crystoballite during calcination at 450 °C,[21] but such phase transition was not observed in this work. The PXRD pattern of used CoAPO-34 catalyst that had been calcined at 580 °C before its MTO reaction at 400 °C still matched well with a CHA and showed no diffraction peak corresponding to dense crystoballite phase. (not shown)

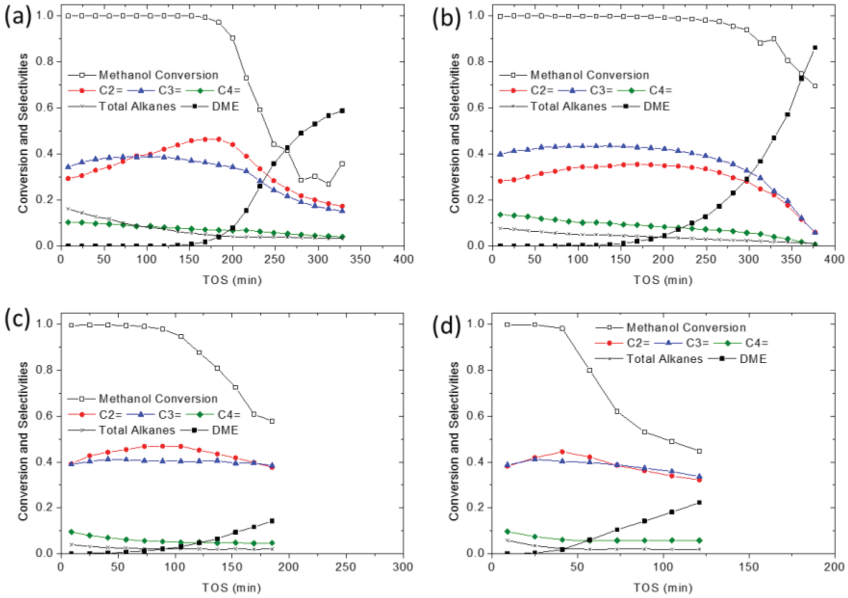

Figure 2.12. MTO-reaction time-on-stream profiles of (a) SSZ-13, (b) SAPO-34, (c) CoAPO-34, and (d) MgAPO-34.

AFX and SFW belong to the ABC-6 class, just like CHA, but have longer cages. Low-silica SSZ-16 and SSZ-52 showed very similar MTO behaviors (Figures 2.13(b–d)) and high-silica SSZ-16 (Figures 2.13(a)) also showed light olefin selectivities very similar to them, except for the initial alkane (propane) selectivity. From these zeolites, ethylene and propylene selectivities started with low values (ca. 10 %) but increased to approximately 35 % at the onset of catalyst deactivation.

The formation of propane particularly noticeable during the initial stage of reaction is known to have close correlation with the formation of polycyclic aromatics. High-silica SSZ-16 showed a lower initial propane selectivity (47.2 %) than that of low-silica SSZ-16 (68.9 %), and this result is consistent with the data observed from a series of SSZ-13 having different Si/Al ratios.[64] SSZ-52 showed the highest initial propane selectivity (71.5 %) among all catalysts demonstrated in this work. Also, SAPO-56 and STA-18 showed the highest values of initial propane selectivities (14.8 % and 19.5 %, respectively) among all $AlPO_4$-based molecular sieves tested here. Interestingly, all AFX and SFW-type molecular sieves demonstrated transient light olefin selectivities very similar to those of CHA-type materials shown above, even though they have much longer cages. One can discern that ethylene selectivity curves are almost overlapped onto propylene selectivity curves, implying that ethylene selectivity is almost equal to propylene selectivity at all stages of reaction.

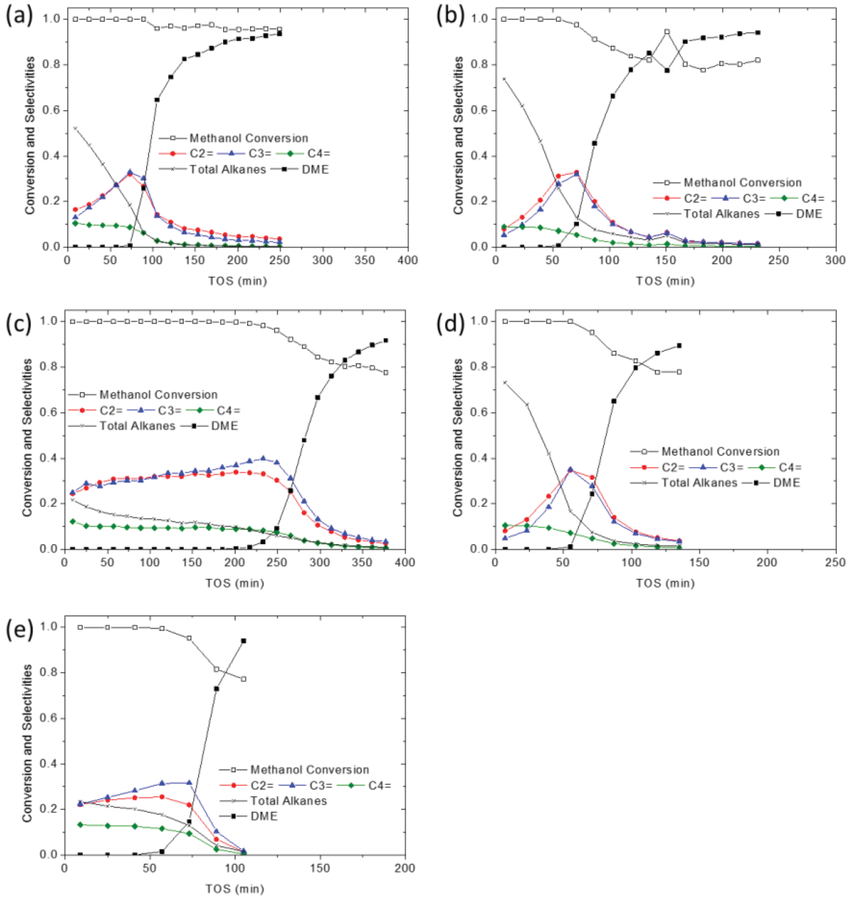

Figure 2.13. MTO-reaction time-on-stream profiles of (a) high-silica SSZ-16, (b) low-silica SSZ-16, (c) SAPO-56, (d) SSZ-52, and (e) STA-18.

SSZ-99 and SSZ-104 are another two zeolites having topologies crystallographically related to CHA. Since these materials have GME-type domains intergrown within the CHA frameworks, it can be said that these two zeolites have much “longer” cages than AFX or SFW, although they are not crystallographically well-defined. SSZ-99 and SSZ-104 showed relatively short lifetimes due to their low Si/Al ratios (3.7 and 3.6, respectively). Also, the initial propane selectivities were high (59.8 % and 59.6 %, respectively), which must be results in consistent with data observed from low-silica CHA having a high density of paired sites.[64]

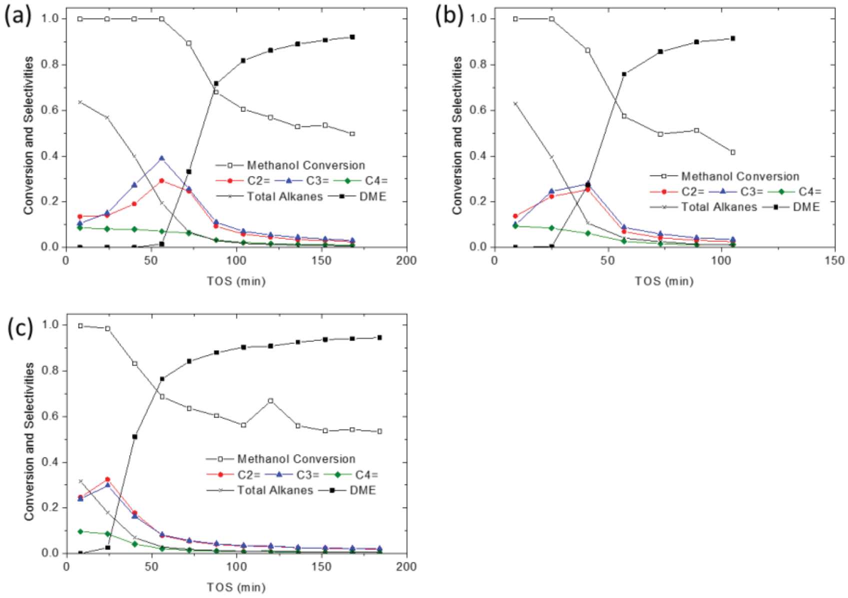

Figure 2.14. MTO-reaction time-on-stream profiles of (a) SSZ-99, (b) SSZ-104, and (c) SSZ-27.

SSZ-27 is the only zeolite that has a one-dimensional channel system among all tested catalysts in this work. Even though a cage can possess a hydrogen pool intermediate, if the presence of such bulky molecules impede the intracrystalline transport of reactants and products, the catalyst will deactivate quickly. Deimund et al. showed that frameworks having low dimension channel systems have shorter lifetimes and lower amounts of coke build-up than materials (SSZ-13 and SAPO-34) with 3-dimensional channel connectivity.[87] Presumably due to the highly tortuous one-dimensional channel, SSZ-27 showed a poor lifetime despite its moderately high Si/Al ratio (14.7).

The LEV framework has the smallest cage among all topologies demonstrated in this work. MTO reaction data of two zeolites (Nu-3 and DMDABCO-LEV) and SAPO-35 were illustrated in Figures 2.15(a–c). The zeolites having LEV topology produced higher ethylene selectivities than propylene. Nu-3 having a higher Si/Al ratio (17.7) showed a longer lifetime than DMDABCO-LEV (Si/Al = 8.3). These results are in coherence with the result of AFX shown above and the study on SSZ-13 by Deimund et al.[64] SAPO-35 yielded more propylene than ethylene, but the ethylene-to-propylene ratio was increased over time of stream. This result is consistent with the previously reported results in literature.[38-39] The short lifetimes of DMDABCO-LEV zeolite and SAPO-35 seem to be results of the cooperation of high acid-site density and 2-dimensional channel system of LEV.

SSZ-98 ERI showed very high ethylene selectivity, and the ethylene-to-propylene ratio also sharply rose over time. This ratio reached the maximum at the beginning of catalyst deactivation. A transient value of 2.07 was recorded at 95 % of methanol conversion. Another ERI-related intergrown zeolite, SSZ-105 has both ERI and LEV cages cooperating in a single catalyst, and also produced ethylene with very high selectivity. The ethylene-to-propylene ratio reached 2.59 at 98% of methanol conversion, and the overall transient behaviors of olefin selectivities resembled the case of SSZ-98. This implies that the presence of the ERI-type cage is responsible for the high ethylene selectivity in the MTO reaction of related zeolites.

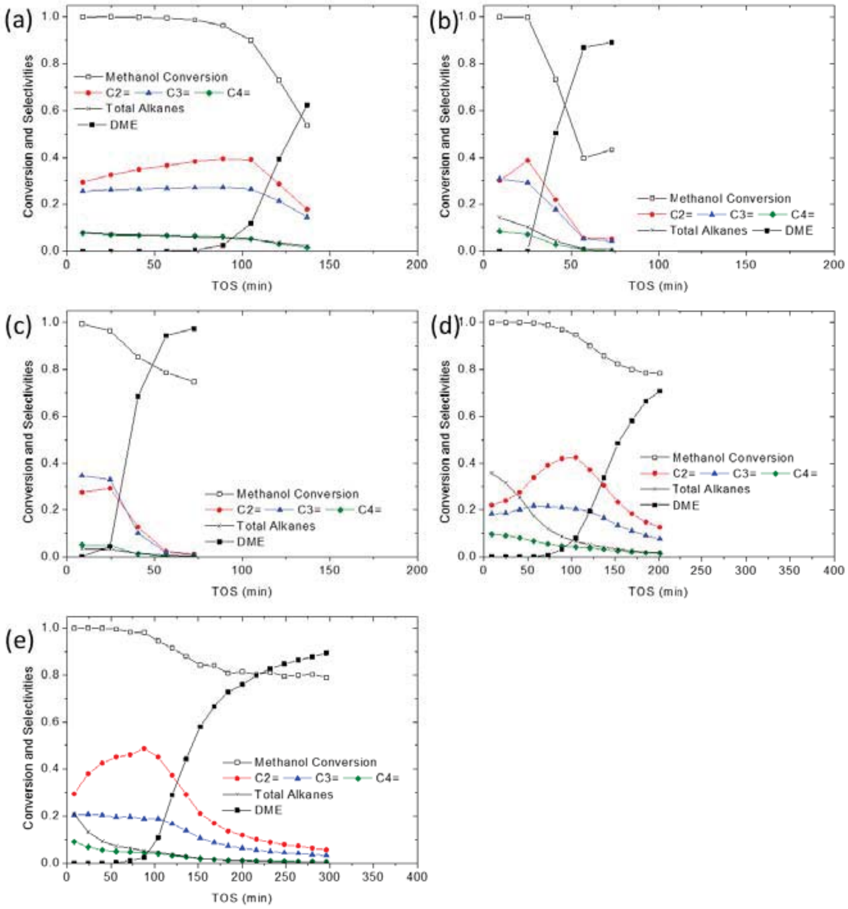

Figure 2.15. MTO-reaction time-on-stream profiles of (a) Nu-3, (b) DMDABCO-LEV, (c) SAPO-35, (d) SSZ-98, and (e) SSZ-105.

Similarly to the case of CHA-type catalysts, zeolite SSZ-39 and three $AlPO_4$-based molecular sieves (SAPO-18, CoAPO-18, and MgAPO-18) were tested for the AEI topology. The MTO results of these AEI-type catalysts were separately reported by others,[46, 67, 69, 88-89] and my results shown in Figure 2.16 were consistent with previous results. From all AEI-type catalysts, propylene was obtained as the predominant olefin product throughout all stages of catalysis. SAPO-18 showed the highest transient propylene selectivity of 50.8 %, and the other three AEI materials also produced high levels of propylene with selectivity over 40 %. The lifetime of SAPO-18 was the longest (514 min for 85 % methanol conversion), while SSZ-39 and MgAPO-18 was deactivated the earliest. A high initial propane selectivity (34.3 %) was observed from SSZ-39 presumably due to the presence of paired acid-sites in the zeolitic surface.

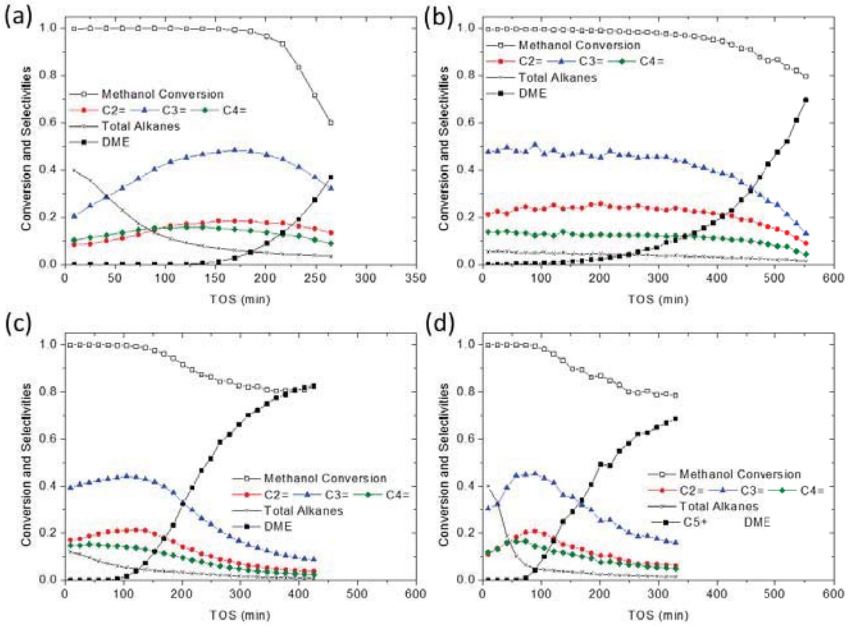

Figure 2.16. MTO-reaction time-on-stream profiles of (a) SSZ-39, (b) SAPO-18, (c) CoAPO-18, and (d) MgAPO-18.

It is noteworthy that the acid strength order of $AlPO_4$-based molecular sieves of AEI framework determined by the NH_3-TPD technique are different to that of CHA. In the case of CHA, SAPO-34 showed the ammonia desorption temperature higher than CoAPO-34 and MgAPO-34, as mentioned above (MAPO-34 < SAPO-34).[20-21] However, it was reported that the ammonia desorption from SAPO-18 occurred at a low temperature (ca. 350 °C), lower than the desorption temperatures of SAPO-34 and other AEI-type catalysts such as MgAPO-18 and CoAPO-18 (SAPO-18 < MAPO-18, SAPO-34).[67, 88, 90] This difference in acidity may have affected each of MTO results of the tested AEI-type catalysts. However, it must be emphasized that, just like the CHA-series, all four AEI-type catalysts showed very similar MTO behaviors, particularly in terms of olefin product distribution.

Figure 2.17 shows MTO data of zeolite RTH and ITE, and two SAV-type SAPO molecular sieves, SAT-7. Similarly to the case of the AEI-type catalysts just shown above, these catalysts also yielded olefin product distributions with predominant propylene selectivities. RTH and ITE are structurally related frameworks having cages which are 2-dimensionally interconnected.[16] Both zeolites showed high propylene selectivities with the lowest transient ethylene-to-propylene ratios lower than 0.5. (0.30 for RTH and 0.42 for ITE) These results are consistent with the literature.[47-48] The high initial propane selectivity of zeolite RTH (47.1 %) which is higher than that of zeolite ITE (26.2 %) seems to be related to its moderately low Si/Al ratio resulting in the more paired Al-sites, given that the cage dimension of the two related topologies are very similar.

SAV is one of the four frameworks (CHA, AEI, SAV and KFI) that are composed only of the d6r units.[16] Here, MTO behaviors of two STA-7 catalysts having different Si contents (Si/T = 0.133, denoted as STA-7(1); Si/T = 0.185, denoted as STA-7(2)) were investigated. The olefin product distributions and lifetimes of these SAV-type catalysts did not show a significant correlation to Si contents. It was previously reported that olefin product distributions from MTO reactions of SAV-type catalysts have a weak correlation to the acid-site density by Pinilla-Herrero et al.[38] STA-7(2) showed an initial propane selectivity (11.5 %) higher than that of STA-7(1) (8.9 %). Since no islanded-Si site was detected in the ^{1}H-decoupled ^{29}Si NMR spectra (not shown) of these SAV-type catalysts, the initial propane selectivities of these STA-7 samples must be explained on the basis of another reason other than the concentration of paired acid sites.

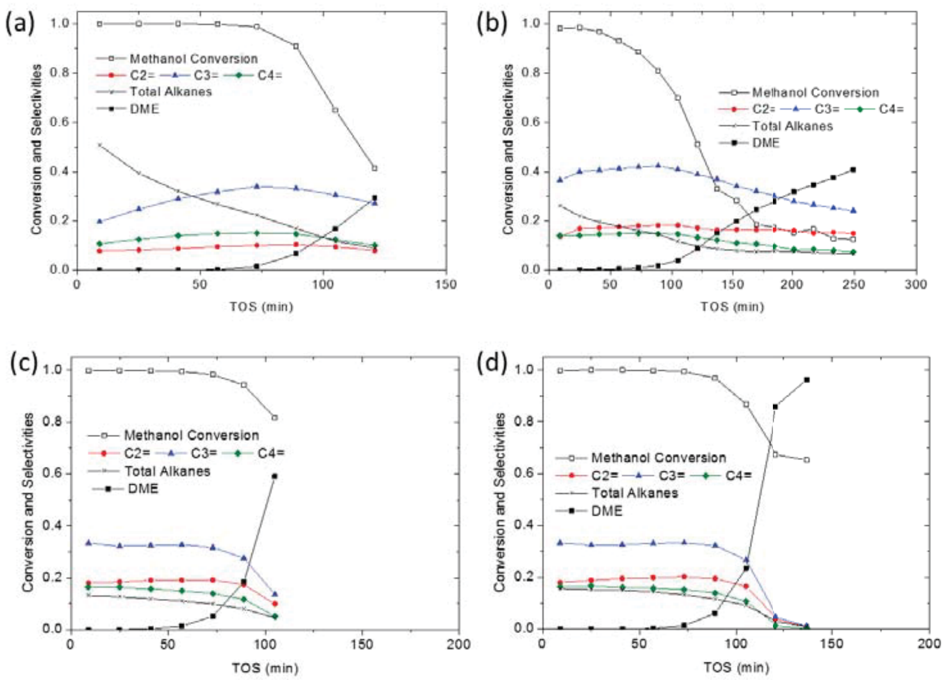

Figure 2.17. MTO-reaction time-on-stream profiles of (a) Zeolite RTH, (b) Zeolite ITE, (c) STA-7(1), and (d) STA-7(2).

The last group of catalysts investigated in this work is the group of LTA, RHO, KFI, and UFI. Unlike the other catalysts shown above, molecular sieves belonging to this group did not show any consistency regarding the ethylene-to-propylene ratios. Zeolite LTA and DNL-6 showed almost 1:1:1 selectivity ratios for ethylene, propylene, and butylenes. While zeolite RHO and KFI showed ethylene selectivities higher than propylene selectivities, SAPO-42 and STA-14 preferably converted methanol to propylene rather than ethylene. UZM-5 was deactivated quickly due to its low dimensionality (2D) of channel connectivity and low Si/Al ratio. These complex patterns shown by this group of molecular sieves will be discussed in the next chapter.

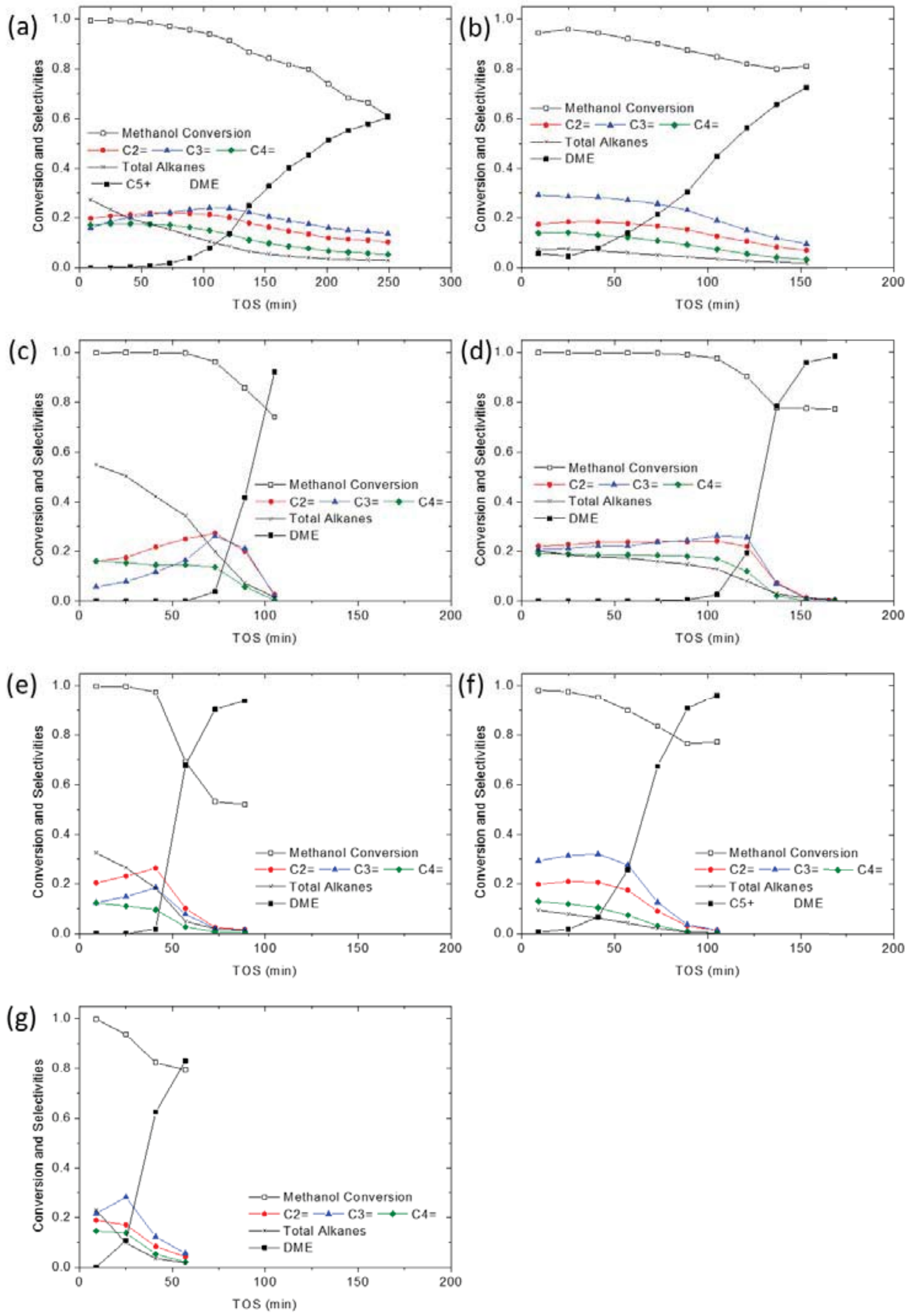

Figure 2.18. MTO-reaction time-on-stream profiles of (a) Zeolite LTA, (b) SAPO-42, (c) Zeolite RHO, (d) DNL-6, (e) Zeolite KFI, (f) STA-14, and (g) UZM-5.

2.4. Summary

In this chapter, the synthesis procedures of molecular sieves studied in this work and OSDAs used to prepare those molecular sieves were provided. The prepared molecular sieves were characterized based on PXRD, SEM and EDS to investigate their crystallinities, morphologies and elemental compositions. The MTO reaction data of the 30 molecular sieves were acquired, and the time-on-stream charts showing transient behaviors of MTO product selectivities were demonstrated. Regardless of elemental compositions, molecular sieves having the same topology showed very similar patterns of selectivities. Some topologies generated more propylene than ethylene, and some others showed ethylene-dominant selectivity patterns. Topologies like CHA, AFX, and SFW gave ethylene selectivities similar to propylene selectivities. Catalysts having LTA cages as their major cages showed very complex patterns of MTO product distributions. Also, catalysts having high concentrations of heteroatom (acid sites) showed high initial propane selectivities.

On the basis of the observation that the topology is more influential to the MTO product distributions than is the element composition, the studied topologies could be classified into four groups: ethylene similar to propylene, higher ethylene, higher propylene, and high butylenes. In the next chapter, the details of this categorization will be dealt with, and a new geometric factor which can correlate the cage geometry to the product distribution will be finally introduced.